NANO LETTERS

pubs.acs.org/NanoLett

Letter

# Nanoscopic Visualization of Restricted Nonvolume Cholinergic and Monoaminergic Transmission with Genetically Encoded Sensors

Paula K. Zhu, W. Sharon Zheng, Peng Zhang, Miao Jing, Philip M. Borden, Farhan Ali, Kaiming Guo, Jiesi Feng, Jonathan S. Marvin, Yali Wang, Jinxia Wan, Li Gan, Alex C. Kwan, Li Lin, Loren L. Looger, Yulong Li, and Yajun Zhang*

Cite This: https://dx.doi.org/10.1021/acs.nanolett.9b04877

Read Online

ACCESS | Metrics & More | Article Recommendations | Supporting Information

**ABSTRACT:** How neuromodulatory transmitters diffuse into the extracellular space remains an unsolved fundamental biological question, despite wide acceptance of the volume transmission model. Here, we report development of a method combining genetically encoded fluorescent sensors with high-resolution imaging and analysis algorithms which permits the first direct visualization of neuromodulatory transmitter diffusion at various neuronal and non-neuronal cells. Our analysis reveals that acetylcholine and monoamines diffuse at individual release sites with a spread length constant of ~0.75 $\mu$m. These transmitters employ varied numbers of release sites, and when spatially close-packed release sites coactivate they can spillover into larger subcellular areas. Our data indicate spatially restricted (i.e., nonvolume) neuromodulatory transmission to be a prominent intercellular communication mode, reshaping current thinking of control and precision of neuromodulation crucial for understanding behaviors and diseases.

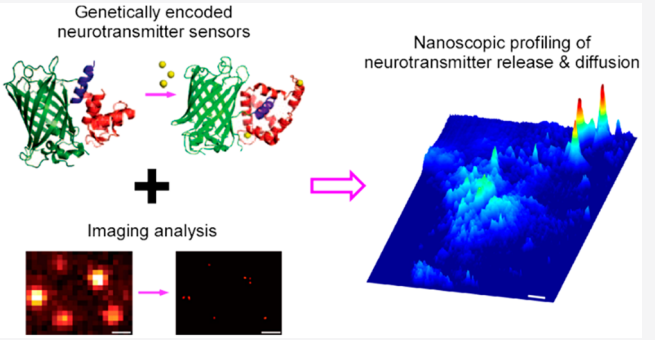


**KEYWORDS:** *Acetylcholine, deconvolution microscopy, genetically encoded fluorescent sensor, norepinephrine, synaptic transmission, volume transmission*



It was proposed three decades ago that the synaptically released, fast neurotransmitters glutamate and gamma-aminobutyric acid (GABA), confined presumably by glial cell barriers, typically mediate one-to-one synaptic transmission, whereas extrasynaptically released neuromodulators, assumed to be less restrained in diffusion and slower in uptake and degradation, mediate one-to-many volume transmission.[1,2] This theory postulates that the primary mode of intercellular neuromodulatory communication is the volume transmission that takes place among cells in general regions, rather than between specific cells that form direct circuits or contacts. Specifically, this model purports that acetylcholine (ACh) and monoamines diffuse into local areas, affecting many different types of nearby cells with neuropeptides traveling even farther and influencing both local cells and distant cells millimeters away.[1,3] The volume transmission theory has gained acceptance over time[3,4] despite lack of supporting evidence and results from multiple combined experimental and simulation studies implicating the contrary.[5−9] Currently, directly examining how endogenous neuromodulatory transmitters diffuse into the extracellular space under physiological conditions remains a technical challenge, because existing imaging approaches do not allow direct visualization of neuromodulatory transmitter release and diffusion at individual release sites.[10,11]

We developed a method that combines genetically encoded fluorescent neuromodulator sensors[12−18] with imaging and analysis algorithms to evaluate spatial diffusion of endogenously released neuromodulatory transmitters, including ACh and monoamines. This analysis produced the first direct visualization of cholinergic and monoaminergic transmission. High-resolution imaging revealed, among other results, isolated putative release sites presynaptic to neuronal (i.e., medial entorhinal stellate, amygdala, locus coeruleus, lateral geniculate, and striatum neurons) and non-neuronal cells (i.e., medial entorhinal astrocytes, and pancreatic and adrenal cells). Quantitative analysis yielded cholinergic and monoaminergic transmitter spread length constants of ~0.75 $\mu$m and defined nanoscopic spatial diffusion profiles of these transmitters at both neuronal and non-neuronal cell sites. These results illustrate that, like fast transmitters glutamate and GABA, neuro-

**Received:** November 24, 2019
**Revised:** April 18, 2020

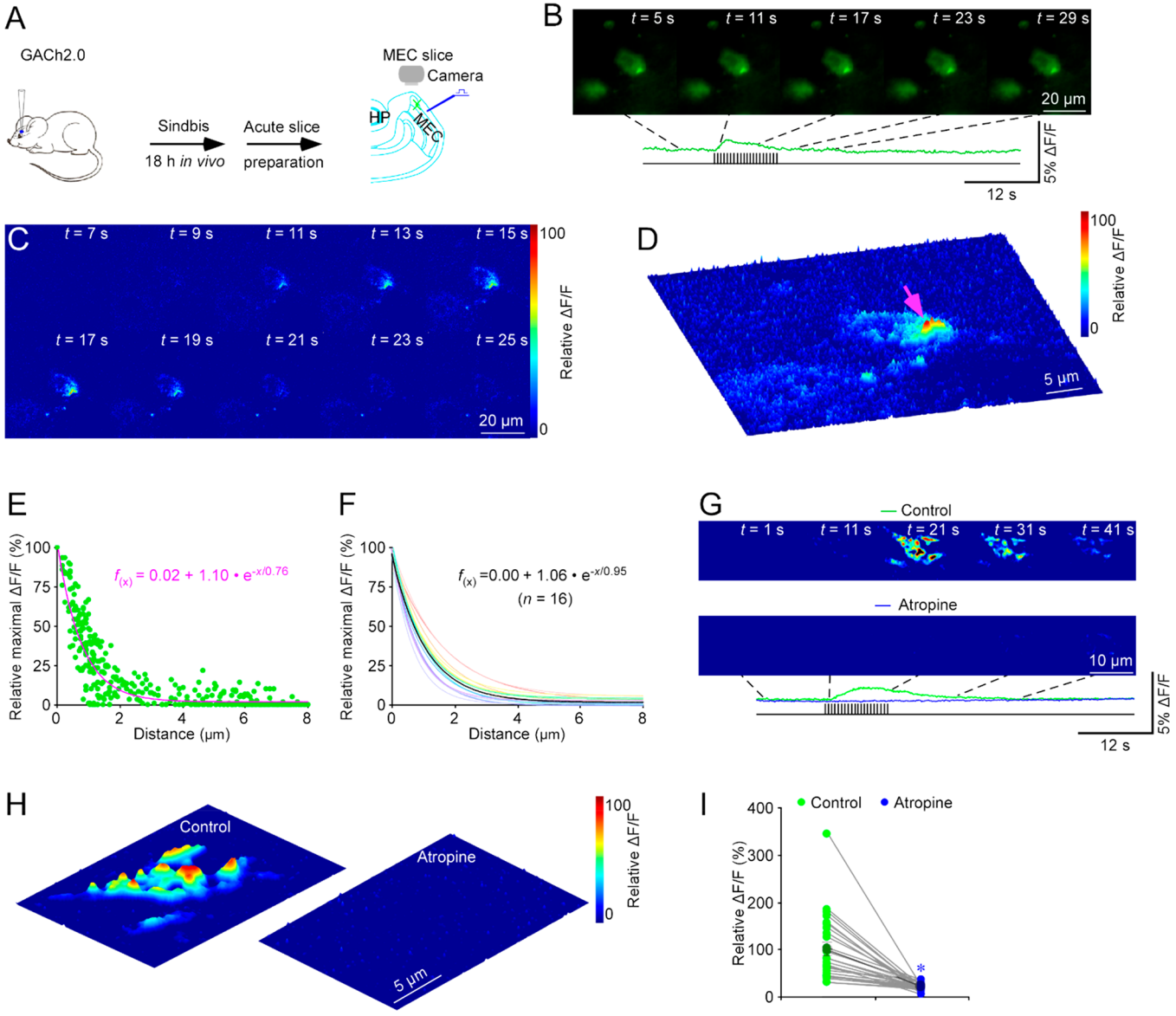


**Figure 1.** GACh2.0 spatiotemporally profiles cholinergic transmission at MEC stellate neurons. (A) Schematic drawing of the design of stimulation-imaging experiments in acute mouse MEC slices. HP, hippocampus; MEC, medial entorhinal cortex. (B–D) Snapshots of fluorescence $\Delta F/F$ responses (B), heatmap displays of time-dependent spatial $\Delta F/F$ responses (C), and three-dimensional spatiotemporal $\Delta F/F$ profiling (D) of a GACh2.0 expressing entorhinal stellate cell in response to local electrical stimuli. Note one isolated release site indicated by the pink arrow in panel D. (E) Pixel-wise maximal $\Delta F/F$ plot at the isolated release site indicated by the pink arrow in panel D. Fitting the data points in this plot with a single exponential decay function (pink line) yields an estimated ACh spread length constant of 0.76 $\mu$m. (F) Summary plot of volume spread length constants obtained from putative single release sites and the average volume spread length constant of 0.95 ± 0.07 $\mu$m for cholinergic transmission at entorhinal stellate neurons ($n$ = 16 from 6 neurons from 5 animals). Note the average single exponential decay function fitting curve in black. (G) Heatmap snapshots of time-dependent spatial $\Delta F/F$ responses of a GACh2.0 expressing entorhinal stellate neuron in response to local electrical stimuli in the normal bath solution and bath solution containing 10 $\mu$M atropine. (H) Heatmap displays of three-dimensional spatiotemporal $\Delta F/F$ profiling of the same GACh2.0 expressing entorhinal stellate neuron in response to local electrical stimuli in the normal bath solution and bath solution containing atropine. (I) Values of peak $\Delta F/F$ responses of putative single release sites measured in the normal bath solution and bath solution containing atropine (Control, 100.0 ± 13.1%; Atropine, 21.5 ± 1.5%; $n$ = 27 from 6 neurons from 6 animals; $Z = -4.541$, $p < 0.005$). Large gray dots indicate average responses and asterisk indicates $p < 0.05$ (Wilcoxon Rank Sum test).

modulatory transmitters use restricted nonvolume transmission as a prominent mode for intercellular communication. These insights into the control and precision of cholinergic and monoaminergic transmission have implications for mechanistic understanding of various behaviors and diseases.

## RESULTS

To profile cholinergic transmission, we made Sindbis viral expression of a G protein-coupled receptor-based genetically encoded fluorescent ACh sensor, GACh2.0,[12] in layer 2 (L2) stellate neurons of the medial entorhinal cortex (MEC) in intact mice and then prepared acute entorhinal slices after ~18 h of *in vivo* expression (Figure 1A). In acute entorhinal slices, we electrically stimulated MEC L1 that is densely innervated by


https://dx.doi.org/10.1021/acs.nanolett.9b04877
Nano Lett. XXXX, XXX, XXX−XXX

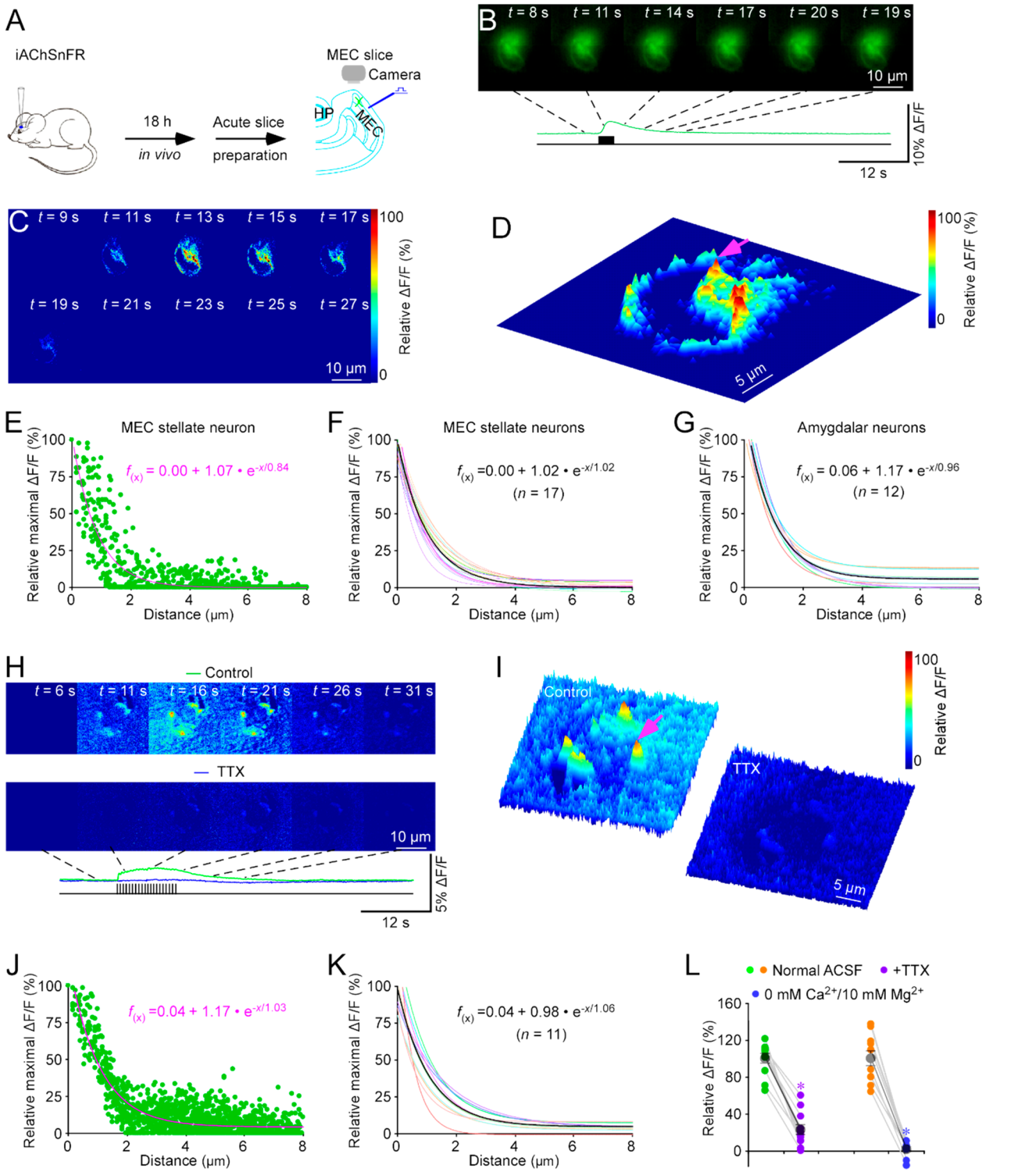


**Figure 2.** iAChSnFR spatiotemporally profiles cholinergic transmission at MEC stellate cells. (A) Schematic drawing of the design of stimulation-imaging experiments in acute mouse MEC slices. HP, hippocampus; MEC, medial entorhinal cortex. (B–D) Snapshots of fluorescence $\Delta F/F$ responses (B), heatmap displays of time-dependent spatial $\Delta F/F$ responses (C), and three-dimensional spatiotemporal $\Delta F/F$ profiling (D) of an iAChSnFR expressing entorhinal stellate neuron in response to local electrical stimuli. Note fluorescence $\Delta F/F$ responses imaged at ~180 nm/pixel resolution (with 40× objective) in panels B–D and one isolated release site indicated by pink arrow in panel D. (E) Pixel-wise maximal $\Delta F/F$ plot at the isolated release site indicated by pink arrow in panel D. Fitting the data points in this plot with a single exponential decay function (pink line) yields an estimated ACh spread length constant of 1.02 $\mu$m. (F) Summary plot of volume spread length constants obtained from putative single release sites and the average volume spread length constant of 1.02 ± 0.05 $\mu$m for cholinergic transmission at entorhinal stellate neurons ($n$ = 17 from 8 neurons from 8 animals). Note the average single exponential decay function fitting curve in black. (G) Summary plot of volume spread length constants obtained from putative single release sites and the average ACh spread length constant of 0.96 ± 0.02 $\mu$m for cholinergic transmission at amygdalar neurons ($n$ = 12 from 4 neurons from 4 animals). Note the average single exponential decay function fitting curve in black. (H) Heatmap snapshots of time-dependent spatial $\Delta F/F$ responses of an iAChSnFR expressing entorhinal stellate cell in response to local electrical stimuli in the normal bath


https://dx.doi.org/10.1021/acs.nanolett.9b04877
Nano Lett. XXXX, XXX, XXX−XXX

**Figure** 2. continued

solution and bath solution containing 1 $\mu$M TTX. (I) Heatmap displays of three-dimensional spatiotemporal $\Delta F/F$ profiling of the same iAChSnFR expressing entorhinal stellate cell in response to local electrical stimuli in the normal bath solution and bath solution containing TTX. Note fluorescence $\Delta F/F$ responses with higher noise when imaged at ~120 nm/pixel resolution (with 60× objective) in panels H and I and one isolated release site indicated by the pink arrow in panel I. (J) Pixel-wise maximal $\Delta F/F$ plot at the isolated release site indicated by the pink arrow in panel I. Fitting the data points in this plot with a single exponential decay function (pink line) yields an estimated ACh spread length constant of 1.03 $\mu$m. (K) Summary plot of volume spread length constants obtained from putative single release sites and the average ACh spread length constant of 1.06 ± 0.09 $\mu$m for cholinergic transmission at entorhinal stellate neurons ($n$ = 11 from 7 neurons from 4 animals). Note the average single exponential decay function fitting curve in black. (L) Values of peak $\Delta F/F$ responses measured in the normal ACSF bath solution and ACSF containing TTX (Control, 100.0 ± 5.0%; TTX, 22.2 ± 5.2%; $n$ = 11 from 4 animals; $Z$ = −3.059, $p$ = 0.002) or 0 mM $Ca^{2+}$/10 mM $Mg^{2+}$ ACSF (Control, 100.0 ± 8.4%; 0 mM $Ca^{2+}$/10 mM $Mg^{2+}$, 1.3 ± 2.3%; $n$ = 10 neurons from 5 animals; $Z$ = −2.803, $p$ = 0.005). Large gray dots indicate average responses and asterisks indicate $p$ < 0.05 (Wilcoxon Rank Sum tests).

cholinergic fibers originating from the basal forebrain[19] and measured fluorescence responses ($\Delta F/F$) of GACh2.0 expressing neurons. Application of 20 pulses of electrical stimuli at 2 Hz induced robust $\Delta F/F$ responses in GACh2.0 expressing neurons (Figure 1B). The $\Delta F/F$ responses of fluorescent transmitter sensor expressing cells exhibited a weak correlation with the basal fluorescence F (Figure S1A,B), suggesting $\Delta F/F$ responses to be largely independent of GACh2.0 expression levels (cf. ref 12). We developed MATLAB-based signal-processing algorithms to analyze the evoked $\Delta F/F$ responses (Figure 1C−D; Methods). The analysis revealed that the evoked $\Delta F/F$ responses were restricted to subcellularly isolated areas, frequently forming clusters of individually isolated release sites (Figure 1D; Movie S1). Pixel-wise maximal $\Delta F/F$ plots at single isolated release sites revealed the spatial spread of cholinergic responses (Figure 1E). Fitting with a single exponential decay function yielded an ACh spread length constant of ~1.0 $\mu$m at entorhinal stellate neurons (Figure 1F). To confirm the cholinergic nature of $\Delta F/F$ responses at single release sites, we included atropine, an inhibitor of GACh2.0[12] (and endogenous muscarinic ACh receptors), in the bath solution (Figure 1G). Bath application of atropine largely eliminated $\Delta F/F$ responses at single release sites (Figure 1H,I), confirming the spatially restricted fluorescence responses to be cholinergic.

We wished to independently verify the cholinergic nature of the evoked signals at entorhinal stellate neurons. Hence, we expressed a bacterial periplasmic binding protein-based genetically encoded fluorescent ACh sensor, iAChSnFR[13,14], in L2 entorhinal stellate neurons in intact mice with Sindbis virus, and after ~18 h of *in vivo* expression imaged $\Delta F/F$ responses in acutely prepared entorhinal slices (Figure 2A). Delivering electrical stimuli at L1 elicited $\Delta F/F$ responses in iAChSnFR expressing neurons with clustered isolated release sites seen at subcellular regions (Figure 2B−D; Movie S2). The image results showed that $\Delta F/F$ responses were largely independent of iAChSnFR expression levels (Figure S1C,D). MATLAB-based algorithms revealed the spatially restricted diffusion of ACh after release, fitting well to a single exponential decay function with a spread length constant of ~1.0 $\mu$m (Figure 2D−F), identical to the spread length constant determined with GACh2.0. We next imaged iAChSnFR expressing neurons in the amygdala and found the same spread length constant of ~1.0 $\mu$m at amygdalar neurons (Figure 2G), suggesting a general spread length constant for ACh.

To validate the analysis method, we performed control experiments with the 40× objective replaced by a higher magnification (60×) objective, which increased the imaging resolution from ~180 to ~120 nm/pixel. Under these conditions, we again recorded the electrically evoked $\Delta F/F$ responses in iAChSnFR expressing entorhinal stellate neurons, yielding a similar ACh spread length constant of ~1.1 $\mu$m (Figure 2H−K; Movie S3). The results rule out potential artifacts that might be introduced during imaging analysis and reconstruction.[20] As a control, we analyzed $\Delta F/F$ responses and basal fluorescence $F$ and found only a weak correlation between them (Figure S1E,F), suggesting $\Delta F/F$ responses to be largely independent of iAChSnFR expression levels. Bath application of tetrodotoxin (TTX), which blocks action potential-evoked synaptic release, diminished the evoked $\Delta F/F$ responses in iAChSnFR expressing entorhinal stellate neurons (Figure 2I,L). Moreover, application of 0 mM $Ca^{2+}$/10 mM $Mg^{2+}$ bath solution, which suppresses all synaptic activities,[21] abolished the evoked $\Delta F/F$ responses in iAChSnFR expressing entorhinal stellate neurons (Figure 2L), confirming the synaptic origin of signals (cf. ref 14). Together, these results indicate that restricted transmission is a common feature of cholinergic signaling on neurons.

We then investigated ACh signals at astrocytes, which express high levels of muscarinic ACh receptors in their fine distal processes involved in tripartite synapses.[22] We used a lentiviral vector carrying a glial fibrillary acidic protein (GFAP) promoter to achieve targeted expression of iAChSnFR in entorhinal astrocytes in mice *in vivo* for ~7 days and then imaged electrically evoked $\Delta F/F$ responses *ex vivo* in acute entorhinal brain slices (Figure 3A). Electric stimuli evoked robust $\Delta F/F$ responses in iAChSnFR expressing astrocytes, and individual, isolated release sites with large $\Delta F/F$ responses were often observed at distal astrocytic processes (Figure 3B,C), illustrating potent cholinergic transmission at astrocytic areas with the highest muscarinic ACh receptor expression.[22] ACh released at these individual sites also had an ACh spread length constant of ~1.0 $\mu$m (Figure 3C−E). Together, these results suggest similarly restricted cholinergic transmission for intercellular communication at both neurons and astrocytes.

We then investigated cholinergic transmission at the pancreas and adrenal gland, in which parasympathetic nerve terminals release ACh to control insulin secretion and to regulate blood pressure and steroid release, respectively.[23,24] We induced Sindbis viral expression of GACh2.0 in the mouse pancreas and adrenal gland *in vivo* and imaged fluorescence responses of GACh2.0 expressing cells in acute pancreatic and adrenal slices after 18 h expression (Figure 3F). Electrical stimulation of local parasympathetic cholinergic fibers evoked $\Delta F/F$ responses in GACh2.0 expressing pancreatic and adrenal cells (Figure 3G,H), confirming our previous report.[12] As with neurons and astrocytes, evoked $\Delta F/F$ responses exhibited clusters of isolated individual release sites at GACh2.0 expressing cells (Figure 3H), and analysis of transmitter diffusion at these release sites gave a


https://dx.doi.org/10.1021/acs.nanolett.9b04877
*Nano Lett.* XXXX, XXX, XXX−XXX

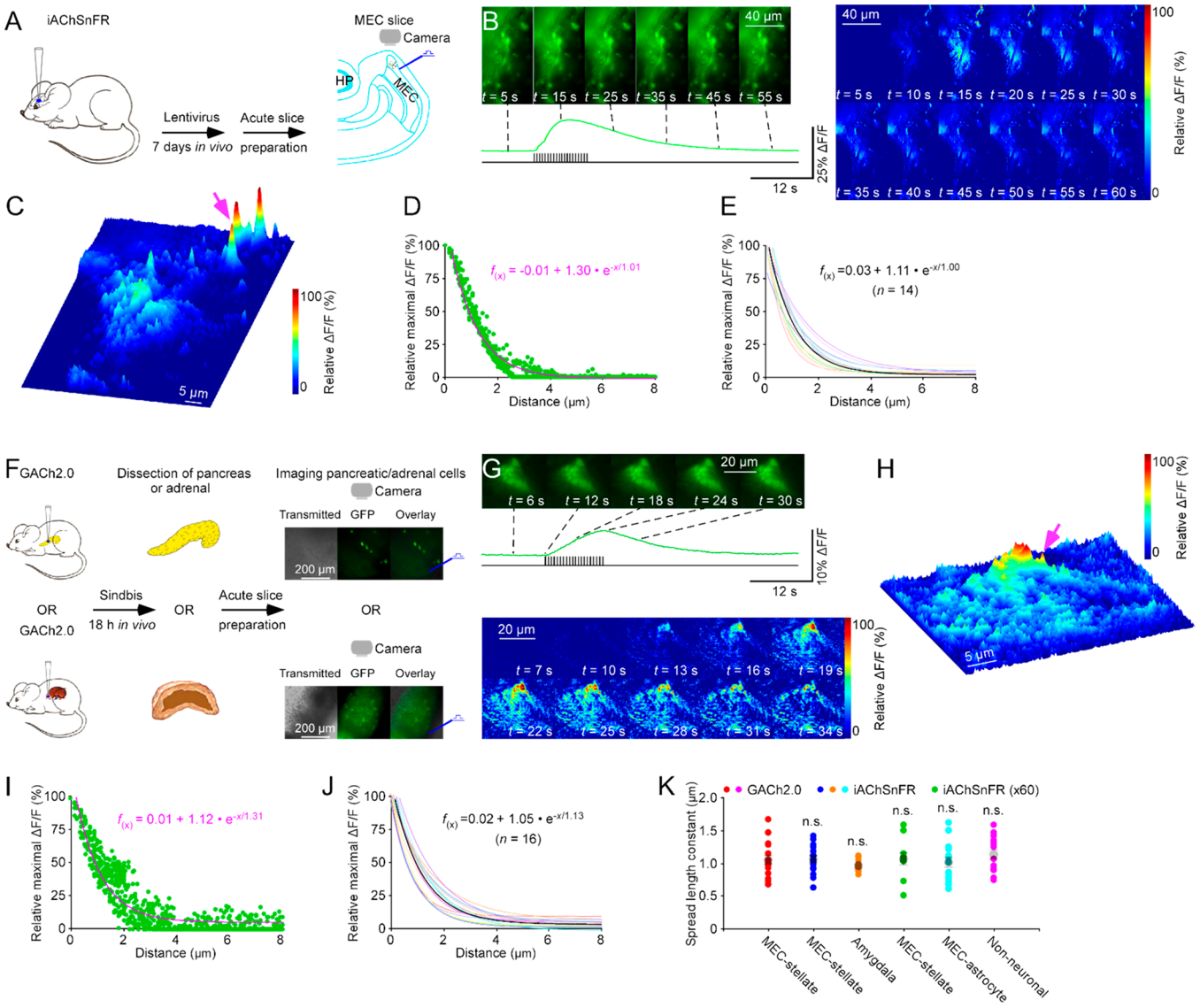


**Figure 3.** ACh sensors spatiotemporally profile cholinergic transmission at non-neuronal cells. (A) Schematic drawing of the design of stimulation-imaging experiments with iAChSnFR in acute mouse MEC slices. HP, hippocampus; MEC: medial entorhinal cortex. (B,C) Snapshots of fluorescence $\Delta F/F$ responses (B left panel), heatmap displays of time-dependent spatial $\Delta F/F$ responses (B right panel), and three-dimensional spatiotemporal $\Delta F/F$ profiling (C) of distal processes of an iAChSnFR expressing entorhinal astrocyte in response to local electrical stimuli. Note one isolated release site indicated by the pink arrow in panel C. Note that the astrocytic cell body, localized below the image, was trimmed to highlight the responses at distal processes. (D) Pixel-wise maximal $\Delta F/F$ plot at the isolated release site indicated by the pink arrow in panel C. Fitting the data points in this plot with a single exponential decay function (pink line) yields an estimated ACh spread length constant of 1.01 $\mu$m. (E) Summary plot of volume spread length constants obtained from putative single release sites and the average volume spread length constant of 1.00 $\pm$ 0.08 $\mu$m for cholinergic transmission at entorhinal astrocytes ($n$ = 14 from 8 neurons from 6 animals). Note the average single exponential decay function fitting curve in black. (F) Schematic drawing of the design of stimulation-imaging experiments with GACh2.0 using an *in vivo* viral expression and *in vitro* mouse pancreatic and adrenal slice preparations. Inserts show transmitted light (left), fluorescence microscopic (middle), and overlay (right) images of GACh2.0 expressing pancreatic and adrenal cells. (G,H) Heatmap snapshots of fluorescence $\Delta F/F$ responses (G upper panel), time-dependent spatial $\Delta F/F$ responses (G lower panel), and three-dimensional spatiotemporal $\Delta F/F$ profiling (H) of a GACh2.0 expressing pancreatic cell in response to local electrical stimuli. Note one isolated release site indicated by the pink arrow in panel H. (I) Pixel-wise maximal $\Delta F/F$ plot at the isolated release site indicated by the pink arrow in panel H. Fitting the data points in this plot with a single exponential decay function (pink line) yields an estimated ACh spread length constant of 1.31 $\mu$m. (J) Summary plot of spread length constants obtained from putative single release sites and the average volume spread length constant of 1.13 $\pm$ 0.07 $\mu$m for cholinergic transmission at the pancreatic and adrenal cells ($n$ = 16 from 8 neurons from 8 animals). Note the average single exponential decay function fitting curve in black. (K) Values for transmitter ACh spread length constants obtained with iAChSnFR at entorhinal stellate neurons ($U$ = 115.0, $p$ = 0.859; see data in Figure 2F), iAChSnFR under 60× objective at entorhinal stellate neurons ($U$ = 74.0, $p$ = 0.505; see data in Figure 2K), iAChSnFR at amygdalar neurons (0.96 $\pm$ 0.02 $\mu$m; $n$ = 12 from 4 neurons from 4 animals; $U$ = 121.0, $p$ = 0.225), iAChSnFR at entorhinal astrocytes ($U$ = 124.0, $p$ = 0.633; see data in panel E), and GACh2.0 at pancreatic and adrenal cells ($U$ = 148.0, $p$ = 0.462; see data in panel J) compared to that obtained with GACh2.0 at entorhinal stellate neurons (Mann−Whitney Rank Sum tests; see data in Figure 1F).

spread length constant of ~1.1 $\mu$m at pancreatic and adrenal cells (Figure 3H−J). Collectively, these data showed no differences in ACh spread length constants at neuronal and non-neuronal cells measured with GACh2.0 and iAChSnFR


https://dx.doi.org/10.1021/acs.nanolett.9b04877
Nano Lett. XXXX, XXX, XXX−XXX

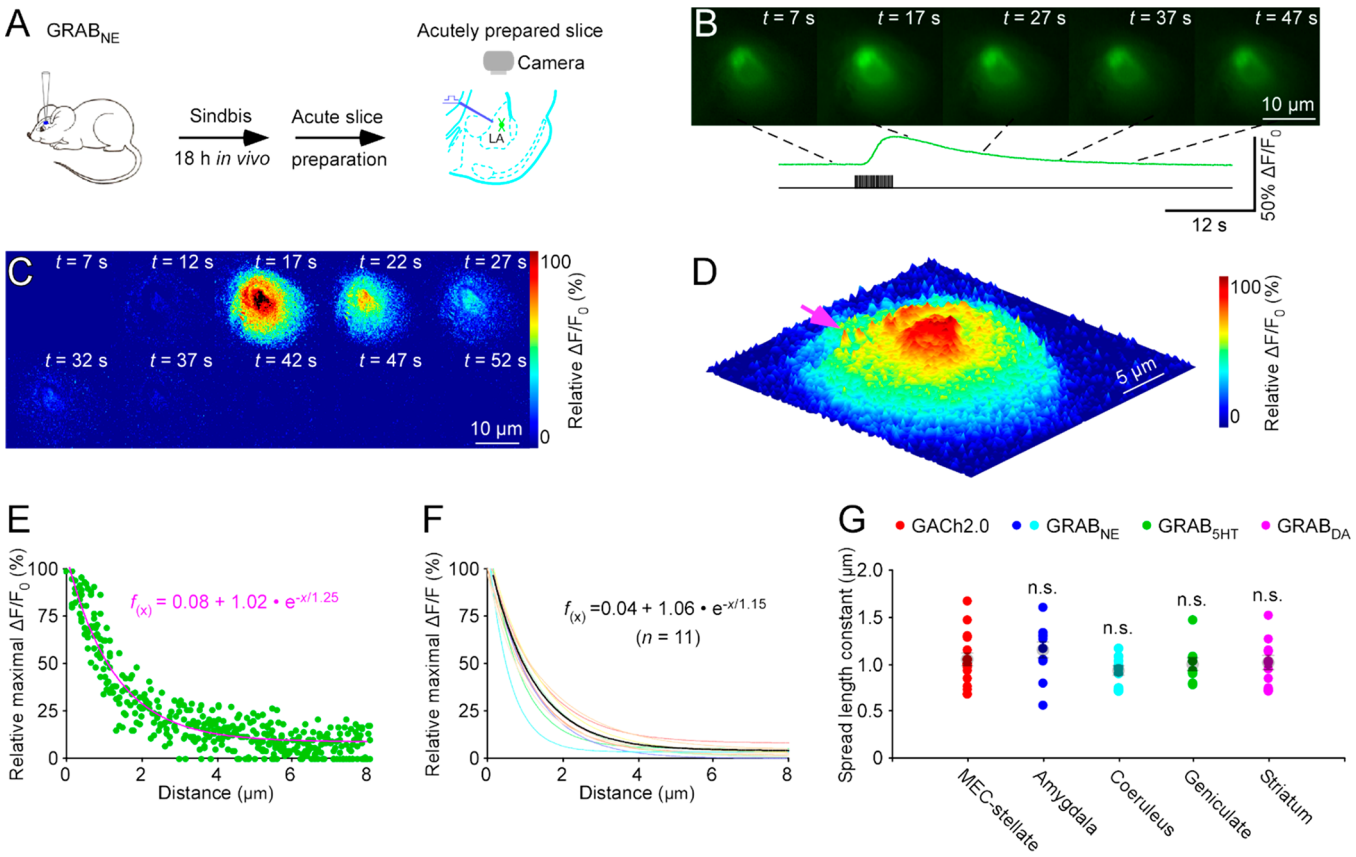


**Figure 4.** GRAB$_{NE1m}$ spatiotemporally profiles adrenergic transmission at amygdalar neurons. (A) Schematic drawing of the design of stimulation-imaging experiments in acute mouse amygdalar slices. LA, lateral amygdala. (B–D) Snapshots of fluorescence $\Delta F/F$ responses (B), heatmap displays of time-dependent spatial $\Delta F/F$ responses (C), and three-dimensional spatiotemporal $\Delta F/F$ profiling (D) of a GRAB$_{NE1m}$ expressing amygdalar neuron to local electrical stimuli. Note one isolated release site indicated by the pink arrow in panel D. (E) Pixel-wise maximal $\Delta F/F$ plot at the isolated release site indicated by the pink arrow in panel D. Fitting the data points in this plot with a single exponential decay function (pink line) yields an estimated NE spread length constant of 1.25 $\mu$m. (F) Summary plot of volume spread length constants obtained from putative single release sites and the average NE spread length constant of 1.15 ± 0.09 $\mu$m for adrenergic transmission at amygdalar neurons ($n$ = 11 from 5 neurons from 5 animals). Note the average single exponential decay function fitting curve in black. (G) Values for monoaminergic transmitter spread length constants obtained with NE sensor at amygdalar neurons ($U$ = 60.0, $p$ = 0.175; see data in Figure 3E) and coerulear neurons (0.92 ± 0.02 $\mu$m; $n$ = 11 from 6 neurons from 6 animals; $U$ = 113.0, $p$ = 0.227), 5HT sensor at geniculate neurons (0.99 ± 0.02 $\mu$m; $n$ = 10 from 7 neurons from 3 animals; $U$ = 88.0, $p$ = 0.693), and DA sensor at striatal neurons (1.00 ± 0.07 $\mu$m; $n$ = 11 from 6 neurons from 6 animals; $U$ = 95.0, $p$ = 0.748) compared to that obtained with GACh2.0 at entorhinal stellate neurons (Mann–Whitney Rank Sum tests; see data in Figure 1F).

sensors at high resolutions (~120 and ~180 nm/pixel) (Figure 3K), supporting the generalization of restricted cholinergic transmission as a major intercellular communication mode for various cell types.

We next examined adrenergic transmission using a genetically encoded fluorescent sensor for norepinephrine (NE), GRAB$_{NE1m}$.[15] We employed Sindbis virus for *in vivo* expression of GRAB$_{NE1m}$ in the mouse amygdala that is heavily innervated by noradrenergic fibers from the locus coeruleus.[25] Approximately 18 h later, we prepared acute amygdalar slices, locally delivered 20 pulses of 4 Hz electrical stimuli, and imaged fluorescence responses of GRAB$_{NE1m}$ expressing neurons (Figure 4A). Electric stimuli evoked slow $\Delta F/F$ responses, typically covering the entire somatic areas of GRAB$_{NE1m}$ expressing amygdalar neurons, although individual isolated release sites were occasionally seen (Figure 4B–D; Movie S4). $\Delta F/F$ responses had only a weak correlation with the basal fluorescence $F$, suggesting the responses to be largely independent of GRAB$_{NE1m}$ expression levels (Figure S1G,H). Spatial diffusion analysis of $\Delta F/F$ responses at isolated single release sites produced an NE spread length constant of ~1.2 $\mu$m at amygdalar neurons (Figure 4D–F), similar in size to spatially restricted postsynaptic adrenergic receptor expression hot spots.[26] To confirm the findings, we imaged GRAB$_{NE1m}$ expressing neurons in the locus coeruleus and found an NE spread length constant of ~0.9 $\mu$m at coerulear neurons (Figure 4G), suggesting a general spread length constant of ~1.0 $\mu$m for NE at different cell types.

Finally, we used the same *in vivo* Sindbis viral expression in the lateral geniculate nucleus and striatum, and subsequent *ex vivo* thalamic and striatal brain slice preparations, to characterize the spatial profiles of two other monoamine transmitters, serotonin (5HT) and dopamine (DA), with genetically encoded fluorescent 5HT and DA sensors, respectively.[16−18] Our analysis of electrically evoked $\Delta F/F$ responses showed that 5HT at geniculate neurons and DA at striatal neurons have the same spread length constant of ~1.0 $\mu$m (Figure 4G). These data are consistent with the idea of restricted nonvolume monoaminergic transmission as a major intercellular communication mode for various neuromodulatory transmitters at different cell types.

To correct for microscopic point-spread function diffraction effects in recorded images, we obtained our microscopic point-


https://dx.doi.org/10.1021/acs.nanolett.9b04877
*Nano Lett.* XXXX, XXX, XXX−XXX

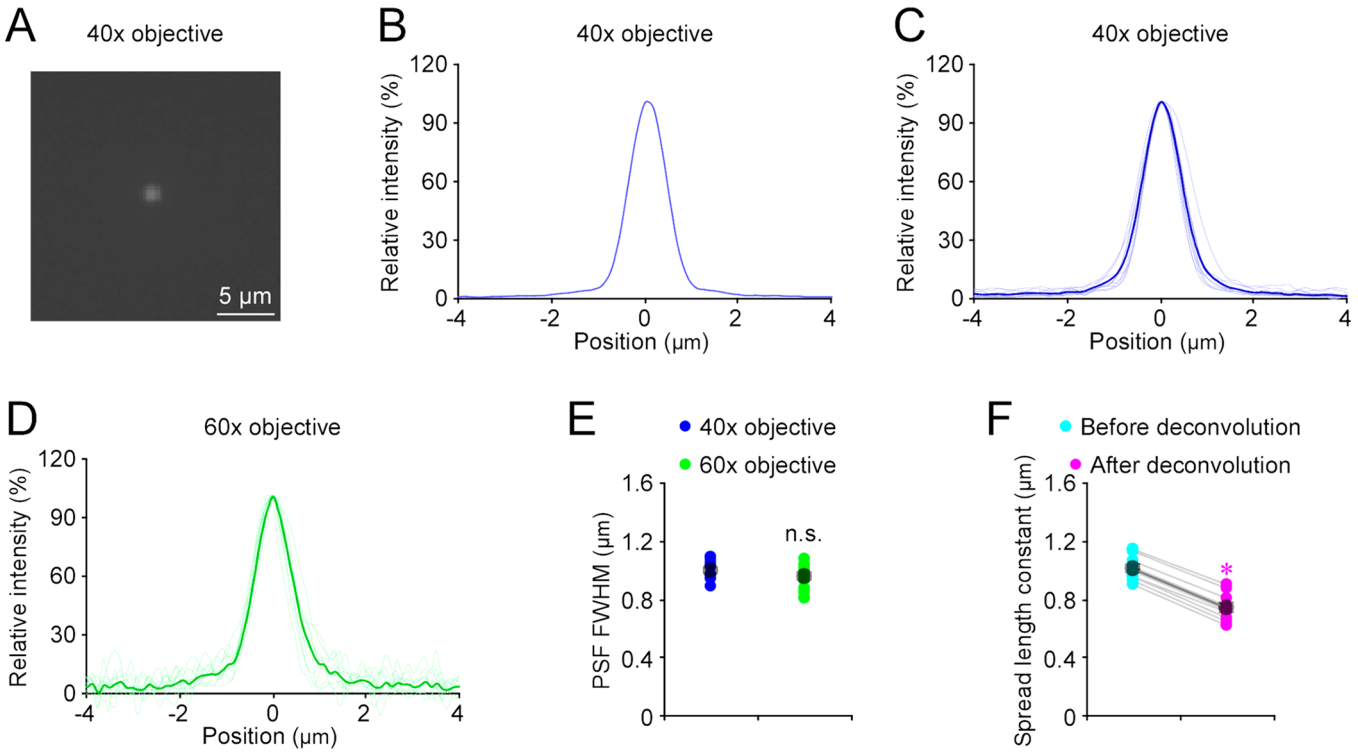


**Figure 5.** Point spread function (PSF) of imaging setup. (A) Fluorescence image of a 23 nm green GATTA bead under a 40× objective. (B) PSF of the 23 nm green GATTA bead shown in panel A obtained under the 40× objective. (C) Individual (light blue) and average (dark blue) PSFs of 23 nm green GATTA beads ($n$ = 10) obtained under the 40× objective. (D) Individual (light green) and average (dark green) PSFs of 23 nm green GATTA beads ($n$ = 10) obtained under the 60× objective. (E) Full width at half maximums (fwhm) of PSFs of 23 nm green GATTA beads ($n$ = 10) obtained under the 40× and 60× objectives (40×, 0.996 ± 0.021 $\mu$m, $n$ = 10; 60×: 0.950 ± 0.027 $\mu$m, $n$ = 10; $U$ = 35.0, p = 0.273; Mann−Whitney Rank Sum test). (F) Diffusion spread length constants before and after deconvolution with measured PSFs (Before, 1.01 ± 0.03; After, 0.74 ± 0.03; $n$ = 10, $Z$ = −2.803, $p$ = 0.005). Asterisk indicates $p < 0.05$ (Wilcoxon Rank Sum test).

spread functions with 23 nm green GATTA beads under both 40× and 60× objectives (Figure 5A−E). Deconvolution based on the measured point-spread functions yielded the true spread length constants of 0.74 ± 0.03 $\mu$m ($n$ = 10 transmitters at various cells) (Figure 5F), indicating ∼35% overestimation before diffraction correction.

## DISCUSSION

In this study, we have developed an imaging and analysis method that permits the first visualization of release and diffusion of endogenous neuromodulatory transmitters and determination of nanoscopic spatial diffusion profiles of these transmitters. These results suggest that highly restricted, nonvolume neuromodulatory transmission is a key mode for intercellular communication between cells in neuronal and non-neuronal tissues; the fine control and precision of cholinergic and monoaminergic signals are likely to be essential for understanding various neuromodulation-mediated behaviors and diseases.

**Restricted versus Volume Transmission.** Visualization of highly restricted cholinergic and monoaminergic transmission directly challenges the prevailing theory of volume transmission of neuromodulators. The volume transmission theory proposes that neuromodulatory transmitters readily diffuse over long distances and affect many different types of nearby cells (in the case of ACh and monoamines) and distant cells millimeters away (in the case of neuropeptides).[1,3] Three decades later, volume transmission remains the dominant theory for neuromodulatory transmission.[3,4] However, the theory is based primarily on the notion that endogenously released neuromodulatory transmitters might behave similarly as exogenously applied ones (that diffuse more freely in the extrasynaptic space), an assumption that has not yet been corroborated by any direct experimental evidence.[8,9]

Over the years, researchers have strived to gauge neurotransmitter diffusion in more quantitative ways. Although previous imaging techniques do not permit direct visualization of endogenous transmitter release and diffusion at individual release sites,[10,11] early studies ingeniously utilized mathematical models to simulate evoked neuromodulatory releases, yielding excellent estimations of transmitter spread areas of ∼5.0−10.0 $\mu$m in diameter.[5−7] However, these studies were underappreciated presumably due to indirect calculation approaches and/or dependence on simulation assumptions. Here, combining super-resolution microscopic analysis strategies[27,28] and genetically encoded sensors,[12−18] we directly visualized and precisely measured diffusion spread length constants of ∼0.75 $\mu$m for both ACh and monoamines, accounting roughly for the previous diffusion area estimations of transmitters that were released presumably from both single and multiple closely spaced release sites.[5−7] These findings support restricted nonvolume neuromodulatory transmission.

**Implications in Physiology.** Our diffusion spread constants specify peak neuromodulatory transmitter concentrations to drop by ∼98% at 5 $\mu$m away from the release sites. Because many genetically encoded neuromodulatory transmitter sensors have affinities comparable to their primogenitors, or endogenous transmitter receptors,[12−18] neuromodulatory transmitters


https://dx.doi.org/10.1021/acs.nanolett.9b04877
Nano Lett. XXXX, XXX, XXX−XXX

released at single sites might induce negligible fluorescent signals and minimal postsynaptic effects in distal areas of the same cells, but not neighboring cells (~15−50 μm away on average), expressing even high-affinity receptors (e.g., $m_2$ muscarinic receptors[29]). Indeed, attention-engaging visual stimulation typically induces reliable ACh release at a few sparse visual cortical neurons, but not their neighbors, in awake mice,[12] providing *in vivo* experimental support. Interestingly, neuromodulatory release sites frequently form well-ordered clusters, mirroring presynaptic neuromodulatory bouton organization,[30] which may be important for superlinear signal summation,[31] signal plasticity,[32,33] and/or fine-tuning of intercellular signals.[34] Obviously, as with the fast transmitters glutamate (e.g., via NMDA receptors[35]) and GABA (e.g., via δ subunit-containing $GABA_A$ receptors[36]), neuromodulatory transmitters may employ high affinity receptors[29,37] and/or large clusters of release sites (Figure 4C,D) to achieve certain volume transmission effects under physiological and pathological conditions.[8,9,14,38,39] Importantly, neuromodulatory transmitter-releasing neurons routinely fire low-frequency action potentials of ~0.02−8 Hz (with average firing rates ≪1 Hz) in intact animals,[40−44] and they release transmitters with low release probabilities and/or strong depression (our unpublished data), indicating that under many physiological conditions, neuromodulatory transmitter release is sparse and low-level. These results suggest that highly restricted transmission with subcellular signal precision is an important mode of neuromodulatory transmission.

Nanoscale pre- and postsynaptic organization is a fundamental determinant of transmission signal amplitude and reliability, and across various synapses the amount of released transmitters, width of synaptic clefts, and location of postsynaptic transmitter receptors all seem to be optimized to maximize synaptic efficacy.[45−47] Here, our visualized spatial diffusion analysis reveals spread length constants of ~0.75 μm for ACh (released synaptically and extrasynaptically[37]) and monoamines at various cell types. Interestingly, the same analysis made on evoked $\Delta F/F$ responses at iGluSnFR[48] expressing amygdalar neurons yields a spread length constant of ~0.62 μm for glutamate (unpublished data; see also ref 49), a slightly smaller value expected for the negatively charged glutamate that can be electrophoretically influenced by excitatory currents.[50] Moreover, we see the same diffusion spread length constant for an endogenously released neuropeptide using a genetically encoded neuropeptide sensor (unpublished data). The similar spread length constants observed across various cell types for fast (e.g., glutamate) and slow transmitters (e.g., ACh, monoamines, and neuropeptide) raises the interesting possibility that transmitter diffusion is optimized across various synapses for transmission efficacy and precision. These results formulate a general concept that both fast (i.e., glutamate and GABA) and neuromodulatory transmitters utilize highly restricted transmission as a key mode of intercellular communication with complementation provided by volume transmission under certain conditions.

**Implications in Diseases.** Highly restricted, nonvolume neuromodulatory transmission explains some perplexing clinical observations and suggests new potential therapeutic interventions. For example, dysregulation of cholinergic transmission is seen in many neurological disorders, including Alzheimer's disease. In fact, the only available therapy for Alzheimer's disease is based on the finding of diminishing ACh release and deteriorating cholinergic neurons in Alzheimer's brains, that is, the cholinergic hypothesis.[51] Currently, all FDA-approved Alzheimer's drugs directly or indirectly inhibit acetylcholinesterase to boost cholinergic signals. These medicines have limited efficacy in cognitive improvement and upon medication termination induce irreversible, accelerated deterioration.[52,53] Our new findings can account for these clinical observations since (1) acetylcholinesterase inhibitors could reduce physiological precision of cholinergic transmission (cf. refs 8 and 9), explaining the only modest cognitive improvement, and (2) long-term application of acetylcholinesterase inhibitors could homeostatically up-regulate acetylcholinesterase levels in Alzheimer's patients and/or down-regulate presynaptic ACh release,[53] explaining the accelerated deterioration upon medication termination. Similarly, impaired adrenergic transmission often appears as the first pathological correlate of cognitive decline in Alzheimer's disease.[54,55] Our results underscore contributions of fine-tuned adrenergic transmission to molding of wakefulness and attention,[34] optimization of behavior in complex social and physical environments,[56,57] and impairment of complex mental tasks (e.g., reasoning and abstract thinking) in Alzheimer's patients.[58] The new insights into cholinergic and adrenergic transmission immediately suggest multiple regulatory mechanisms as potentially effective intervention targets and set the physiological transmission baseline for future medication testing and development.

Dysregulation of central cholinergic and monoaminergic transmission is also linked to other major brain disorders, including addiction,[59,60] autism,[61] epilepsy,[62,63] Parkinson's disease,[64,65] and sleep disorders,[57] as well as a large group of anxiety and mood disorders.[66−68] Moreover, defective cholinergic and monoaminergic signals may underlie pathogenesis of a number of non-neurological diseases, including cardiovascular disease, diabetes, immune deficiency, and tumorigenesis.[69−73] We expect our new method to lead to more comprehensive understanding of fundamental properties and regulation of cholinergic and monoaminergic transmission, which is essential for dissecting pathogenic mechanisms and developing effective interventions for these diseases.

## ■ ASSOCIATED CONTENT

### Supporting Information

The Supporting Information is available free of charge at https://pubs.acs.org/doi/10.1021/acs.nanolett.9b04877.

Methods; Figures S1 and S2 (PDF)

Imaging endogenous acetylcholine release at an entorhinal stellate neuron with GACh2.0 (AVI)

Imaging endogenous acetylcholine release at an entorhinal stellate neuron with iAChSnFR (AVI)

Imaging endogenous acetylcholine release at an entorhinal stellate neuron with iAChSnFR (60x objective) (AVI)

Imaging endogenous norepinephrine release at an amygdalar neuron with $GRAB_{NE1m}$(AVI)

## ■ AUTHOR INFORMATION

### Corresponding Author

**Yajun Zhang** − *State Key Laboratory of Membrane Biology and Peking-Tsinghua Center for Life Sciences, Peking University, Beijing 100871, China; Department of Pharmacology, University of Virginia School of Medicine, Charlottesville, Virginia 22908, United States*; Email: yz6k@virginia.edu



https://dx.doi.org/10.1021/acs.nanolett.9b04877
*Nano Lett.* XXXX, XXX, XXX−XXX

## Authors

**Paula K. Zhu** − *State Key Laboratory of Membrane Biology and Peking-Tsinghua Center for Life Sciences, Peking University, Beijing 100871, China; Math, Engineering, and Science Academy Class of 2020, Albemarle High School, Charlottesville, Virginia 22901, United States; Summer Secondary School Neurobiology Class of 2019, Harvard University, Cambridge, Massachusetts 02138, United States*

**W. Sharon Zheng** − *Department of Pharmacology and Biomedical Engineering Class of 2021, University of Virginia School of Medicine, Charlottesville, Virginia 22908, United States*

**Peng Zhang** − *Department of Pharmacology, University of Virginia School of Medicine, Charlottesville, Virginia 22908, United States*

**Miao Jing** − *State Key Laboratory of Membrane Biology and Peking-Tsinghua Center for Life Sciences, Peking University, Beijing 100871, China; Chinese Institute for Brain Research, Beijing 100871, China*

**Philip M. Borden** − *Janelia Research Campus, Howard Hughes Medical Institute, Ashburn, Virginia 20147, United States*

**Farhan Ali** − *Department of Psychiatry, Yale University School of Medicine, New Haven, Connecticut 06511, United States*

**Kaiming Guo** − *Department of Pharmacology, University of Virginia School of Medicine, Charlottesville, Virginia 22908, United States; School of Pharmaceutical Sciences, Wenzhou Medical University, Wenzhou 325035, China*

**Jiesi Feng** − *State Key Laboratory of Membrane Biology and Peking-Tsinghua Center for Life Sciences, Peking University, Beijing 100871, China*

**Jonathan S. Marvin** − *Janelia Research Campus, Howard Hughes Medical Institute, Ashburn, Virginia 20147, United States;* orcid.org/0000-0003-2294-4515

**Yali Wang** − *Department of Pharmacology, University of Virginia School of Medicine, Charlottesville, Virginia 22908, United States*

**Jinxia Wan** − *State Key Laboratory of Membrane Biology and Peking-Tsinghua Center for Life Sciences, Peking University, Beijing 100871, China*

**Li Gan** − *Helen and Robert Appel Alzheimer's Disease Research Institute, Weill Cornell Medicine College, New York, New York 10065, United States*

**Alex C. Kwan** − *Department of Psychiatry, Yale University School of Medicine, New Haven, Connecticut 06511, United States;* orcid.org/0000-0003-2169-1667

**Li Lin** − *School of Pharmaceutical Sciences, Wenzhou Medical University, Wenzhou 325035, China*

**Loren L. Looger** − *Janelia Research Campus, Howard Hughes Medical Institute, Ashburn, Virginia 20147, United States;* orcid.org/0000-0002-7531-1757

**Yulong Li** − *State Key Laboratory of Membrane Biology and Peking-Tsinghua Center for Life Sciences, Peking University, Beijing 100871, China*

Complete contact information is available at: https://pubs.acs.org/10.1021/acs.nanolett.9b04877


## Author Contributions

P.K.Z. and Y.Z. conceived the concept and led the project with input from L.G., A.C.K., L.L., L.L.L., and Y.L.; P.K.Z. developed MATLAB-based algorithms and analyzed data with assistance from W.S.Z.; P.Z. and Y.Z. performed molecular biology experiments and collected imaging data with assistance from P.K.Z., K.G., F.A., and Y.W.; L.L.L., J.S.M., P.M.B., Y.L., J.M., J.F., and J.W. provided key reagents; P.K.Z. and Y.Z. wrote the manuscript with input from all coauthors.

## Notes

The authors declare no competing financial interest.

## ■ ACKNOWLEDGMENTS

We thank members of the Julius Zhu lab for suggestions and technical support, and Drs. Gerard Borst, Yiyang Gong, Ling-Gang Wu, and Zhuan Zhou for inspirational discussions and critical comments. This study is supported in part by Intel International Science and Engineering Fair Award (P.K.Z.), Harrison Undergraduate Research Award (W.S.Z.), Alzheimer's Association Postdoc-to-Faculty Transitioning Research Fellowships AARF-17-504924 (F.A.) and AARF-19-619387 (P.Z.), National Natural Science Foundation of China Young Scholar Award NSFC81701070 (Y.W.), and a Peking-Tsinghua Center Excellence Postdoctoral Fellowship (Y.Z.).

## ■ REFERENCES


(1) Agnati, L. F.; Bjelke, B.; Fuxe, K. Volume transmission in the brain. *Am. Sci.* **1992**, *80* (4), 362−373.

(2) Zoli, M.; Jansson, A.; Sykova, E.; Agnati, L. F.; Fuxe, K. Volume transmission in the CNS and its relevance for neuropsychopharmacology. *Trends Pharmacol. Sci.* **1999**, *20* (4), 142−50.

(3) Borroto-Escuela, D. O.; Perez De La Mora, M.; Manger, P.; Narvaez, M.; Beggiato, S.; Crespo-Ramirez, M.; Navarro, G.; Wydra, K.; Diaz-Cabiale, Z.; Rivera, A.; Ferraro, L.; Tanganelli, S.; Filip, M.; Franco, R.; Fuxe, K. Brain dopamine transmission in health and Parkinson's disease: modulation of synaptic transmission and plasticity through volume transmission and dopamine heteroreceptors. *Front. Synaptic Neurosci.* **2018**, *10*, 20.

(4) Gundersen, V.; Storm-Mathisen, J.; Bergersen, L. H. Neuroglial transmission. *Physiol. Rev.* **2015**, *95* (3), 695−726.

(5) Beckstead, M. J.; Grandy, D. K.; Wickman, K.; Williams, J. T. Vesicular dopamine release elicits an inhibitory postsynaptic current in midbrain dopamine neurons. *Neuron* **2004**, *42* (6), 939−46.

(6) Courtney, N. A.; Ford, C. P. The timing of dopamine- and noradrenaline-mediated transmission reflects underlying differences in the extent of spillover and pooling. *J. Neurosci.* **2014**, *34* (22), 7645−56.

(7) Courtney, N. A.; Ford, C. P. Mechanisms of 5-HT1A receptor-mediated transmission in dorsal raphe serotonin neurons. *J. Physiol.* **2016**, *594* (4), 953−65.

(8) Barbour, B.; Hausser, M. Intersynaptic diffusion of neurotransmitter. *Trends Neurosci.* **1997**, *20* (9), 377−84.

(9) Sarter, M.; Parikh, V.; Howe, W. M. Phasic acetylcholine release and the volume transmission hypothesis: time to move on. *Nat. Rev. Neurosci.* **2009**, *10* (5), 383−90.

(10) Sykova, E.; Nicholson, C. Diffusion in brain extracellular space. *Physiol. Rev.* **2008**, *88* (4), 1277−340.

(11) Zheng, K.; Jensen, T. P.; Savtchenko, L. P.; Levitt, J. A.; Suhling, K.; Rusakov, D. A. Nanoscale diffusion in the synaptic cleft and beyond measured with time-resolved fluorescence anisotropy imaging. *Sci. Rep.* **2017**, *7*, 42022.

(12) Jing, M.; Zhang, P.; Wang, G.; Feng, J.; Mesik, L.; Zeng, J.; Jiang, H.; Wang, S.; Looby, J. C.; Guagliardo, N. A.; Langma, L. W.; Lu, J.; Zuo, Y.; Talmage, D. A.; Role, L. W.; Barrett, P. Q.; Zhang, L. I.; Luo, M.; Song, Y.; Zhu, J. J.; Li, Y. A genetically encoded fluorescent acetylcholine indicator for in vitro and in vivo studies. *Nat. Biotechnol.* **2018**, *36* (8), 726−737.

(13) Kazemipour, A.; Novak, O.; Flickinger, D.; Marvin, J. S.; Abdelfattah, A. S.; King, J.; Borden, P. M.; Kim, J. J.; Al-Abdullatif, S. H.; Deal, P. E.; Miller, E. W.; Schreiter, E. R.; Druckmann, S.; Svoboda, K.; Looger, L. L.; Podgorski, K. Kilohertz frame-rate two-photon tomography. *Nat. Methods* **2019**, *16* (8), 778−786.

(14) Borden, P. M.; Zhang, P.; Shivange, A. V; Marvin, J. S.; Cichon, J.; Dan, C.; Podgorski, K.; Figueiredo, A.; Novak, O.; Tanimoto, M.; Shigetomi, E.; Lobas, M. A.; Kim, H.; Zhu, P.; Zhang, Y.; Zheng, W. S.; Fan, C.; Wang, G.; Xiang, B.; Gan, L.; Zhang, G.-X.; Guo, K.; Lin, L.; Cai, Y.; Yee, A. G.; Aggarwal, A.; Bao, H.; Lou, X.; Chapman, E. R.;




https://dx.doi.org/10.1021/acs.nanolett.9b04877
*Nano Lett.* XXXX, XXX, XXX−XXX

Ford, C. P.; Rees, D.; Dietrich, D.; Khakh, B. S.; Dittman, J. S.; Gan, W.-B.; Koyama, M.; Jayaraman, V.; Cheer, J. F.; Lester, H. A.; Zhu, J. J.; Looger, L. A fast genetically encoded fluorescent sensor for faithful in vivo acetylcholine detection in mice, fish, worms and flies. *bioRxiv* **2020**, DOI: 10.1101/2020.02.07.939504.

(15) Feng, J.; Zhang, C.; Lischinsky, J. E.; Jing, M.; Zhou, J.; Wang, H.; Zhang, Y.; Dong, A.; Wu, Z.; Wu, H.; Chen, W.; Zhang, P.; Zou, J.; Hires, S. A.; Zhu, J. J.; Cui, G.; Lin, D.; Du, J.; Li, Y. A genetically encoded fluorescent sensor for rapid and specific in vivo detection of norepinephrine. *Neuron* **2019**, *102* (4), 745.

(16) Wan, J.; Peng, W.; Li, X.; Qian, T.; Song, K.; Zeng, J.; Deng, F.; Hao, S.; Feng, J.; Zhang, P.; Zhang, Y.; Zou, J.; Pan, S.; Zhu, J. J.; Jing, M.; Xu, M.; Li, Y. A genetically encoded GRAB sensor for measuring serotonin dynamics *in vivo*. *bioRxiv* **2020**, DOI: 10.1101/2020.02.24.962282.

(17) Patriarchi, T.; Cho, J. R.; Merten, K.; Howe, M. W.; Marley, A.; Xiong, W. H.; Folk, R. W.; Broussard, G. J.; Liang, R. Q.; Jang, M. J.; Zhong, H. N.; Dombeck, D.; von Zastrow, M.; Nimmerjahn, A.; Gradinaru, V.; Williams, J. T.; Tian, L. Ultrafast neuronal imaging of dopamine dynamics with designed genetically encoded sensors. *Science* **2018**, *360* (6396), eaat4422.

(18) Sun, F. M.; Zeng, J. Z.; Jing, M.; Zhou, J. H.; Feng, J. S.; Owen, S. F.; Luo, Y. C.; Li, F. N.; Wang, H.; Yamaguchi, T.; Yong, Z. H.; Gao, Y. J.; Peng, W. L.; Wang, L. Z.; Zhang, S. Y.; Du, J. L.; Lin, D. Y.; Xu, M.; Kreitzer, A. C.; Cui, G. H.; Li, Y. L. A genetically encoded fluorescent sensor enables rapid and specific detection of dopamine in flies, fish, and mice. *Cell* **2018**, *174* (2), 481−96.

(19) Ray, S.; Naumann, R.; Burgalossi, A.; Tang, Q.; Schmidt, H.; Brecht, M. Grid-layout and theta-modulation of layer 2 pyramidal neurons in medial entorhinal cortex. *Science* **2014**, *343* (6173), 891−6.

(20) Small, A.; Stahlheber, S. Fluorophore localization algorithms for super-resolution microscopy. *Nat. Methods* **2014**, *11* (3), 267−79.

(21) McCormack, S. G.; Stornetta, R. L.; Zhu, J. J. Synaptic AMPA receptor exchange maintains bidirectional plasticity. *Neuron* **2006**, *50* (1), 75−88.

(22) Van Der Zee, E. A.; De Jong, G. I.; Strosberg, A. D.; Luiten, P. G. Muscarinic acetylcholine receptor-expression in astrocytes in the cortex of young and aged rats. *Glia* **1993**, *8* (1), 42−50.

(23) Satin, L. S.; Kinard, T. A. Neurotransmitters and their receptors in the islets of Langerhans of the pancreas: what messages do acetylcholine, glutamate, and GABA transmit? *Endocr. J.* **1998**, *8* (3), 213−23.

(24) Ungar, A.; Phillips, J. H. Regulation of the adrenal medulla. *Physiol. Rev.* **1983**, *63* (3), 787−843.

(25) Foote, S. L.; Bloom, F. E.; Astonjones, G. Nucleus locus ceruleus - new evidence of anatomical and physiological specificity. *Physiol. Rev.* **1983**, *63* (3), 844−914.

(26) Sungkaworn, T.; Jobin, M. L.; Burnecki, K.; Weron, A.; Lohse, M. J.; Calebiro, D. Single-molecule imaging reveals receptor-G protein interactions at cell surface hot spots. *Nature* **2017**, *550* (7677), 543−547.

(27) Sauer, M. Localization microscopy coming of age: from concepts to biological impact. *J. Cell Sci.* **2013**, *126* (16), 3505−13.

(28) Li, H.; Vaughan, J. C. Switchable fluorophores for single-molecule localization microscopy. *Chem. Rev.* **2018**, *118* (18), 9412−9454.

(29) Kellar, K. J.; Martino, A. M.; Hall, D. P., Jr.; Schwartz, R. D.; Taylor, R. L. High-affinity binding of [3H]acetylcholine to muscarinic cholinergic receptors. *J. Neurosci.* **1985**, *5* (6), 1577−82.

(30) Liu, C.; Kershberg, L.; Wang, J.; Schneeberger, S.; Kaeser, P. S. Dopamine secretion is mediated by sparse active zone-like release sites. *Cell* **2018**, *172* (4), 706−718.

(31) Larkum, M. E.; Nevian, T. Synaptic clustering by dendritic signalling mechanisms. *Curr. Opin. Neurobiol.* **2008**, *18* (3), 321−31.

(32) Makino, H.; Malinow, R. Compartmentalized versus global synaptic plasticity on dendrites controlled by experience. *Neuron* **2011**, *72* (6), 1001−11.

(33) Fu, M.; Yu, X.; Lu, J.; Zuo, Y. Repetitive motor learning induces coordinated formation of clustered dendritic spines in vivo. *Nature* **2012**, *483* (7387), 92−5.

(34) Carter, M. E.; Yizhar, O.; Chikahisa, S.; Nguyen, H.; Adamantidis, A.; Nishino, S.; Deisseroth, K.; de Lecea, L. Tuning arousal with optogenetic modulation of locus coeruleus neurons. *Nat. Neurosci.* **2010**, *13* (12), 1526−33.

(35) Rusakov, D. A.; Kullmann, D. M.; Stewart, M. G. Hippocampal synapses: do they talk to their neighbours? *Trends Neurosci.* **1999**, *22* (9), 382−8.

(36) Brickley, S. G.; Mody, I. Extrasynaptic $GABA_A$ receptors: their function in the CNS and implications for disease. *Neuron* **2012**, *73* (1), 23−34.

(37) Dani, J. A.; Bertrand, D. Nicotinic acetylcholine receptors and nicotinic cholinergic mechanisms of the central nervous system. *Annu. Rev. Pharmacol. Toxicol.* **2007**, *47*, 699−729.

(38) Seamans, J. K.; Yang, C. R. The principal features and mechanisms of dopamine modulation in the prefrontal cortex. *Prog. Neurobiol.* **2004**, *74* (1), 1−58.

(39) Okaty, B. W.; Commons, K. G.; Dymecki, S. M. Embracing diversity in the 5-HT neuronal system. *Nat. Rev. Neurosci.* **2019**, *20* (7), 397−424.

(40) Simon, A. P.; Poindessous-Jazat, F.; Dutar, P.; Epelbaum, J.; Bassant, M. H. Firing properties of anatomically identified neurons in the medial septum of anesthetized and unanesthetized restrained rats. *J. Neurosci.* **2006**, *26* (35), 9038−9046.

(41) Duque, A.; Tepper, J. M.; Detari, L.; Ascoli, G. A.; Zaborszky, L. Morphological characterization of electrophysiologically and immunohistochemically identified basal forebrain cholinergic and neuropeptide Y-containing neurons. *Brain Struct. Funct.* **2007**, *212* (1), 55−73.

(42) Aston-Jones, G.; Bloom, F. E. Activity of norepinephrine-containing locus coeruleus neurons in behaving rats anticipates fluctuations in the sleep-waking cycle. *J. Neurosci.* **1981**, *1* (8), 876−86.

(43) Cohen, J. Y.; Amoroso, M. W.; Uchida, N. Serotonergic neurons signal reward and punishment on multiple timescales. *eLife* **2015**, *4*, No. e06346.

(44) Grace, A. A.; Bunney, B. S. The control of firing pattern in nigral dopamine neurons: single spike firing. *J. Neurosci.* **1984**, *4* (11), 2866−76.

(45) Savtchenko, L. P.; Sylantyev, S.; Rusakov, D. A. Central synapses release a resource-efficient amount of glutamate. *Nat. Neurosci.* **2013**, *16* (1), 10−2.

(46) Savtchenko, L. P.; Rusakov, D. A. The optimal height of the synaptic cleft. *Proc. Natl. Acad. Sci. U. S. A.* **2007**, *104* (6), 1823−8.

(47) Haas, K. T.; Compans, B.; Letellier, M.; Bartol, T. M.; Grillo-Bosch, D.; Sejnowski, T. J.; Sainlos, M.; Choquet, D.; Thoumine, O.; Hosy, E. Pre-post synaptic alignment through neuroligin-1 tunes synaptic transmission efficiency. *eLife* **2018**, *7*, No. e31755.

(48) Marvin, J. S.; Borghuis, B. G.; Tian, L.; Cichon, J.; Harnett, M. T.; Akerboom, J.; Gordus, A.; Renninger, S. L.; Chen, T. W.; Bargmann, C. I.; Orger, M. B.; Schreiter, E. R.; Demb, J. B.; Gan, W. B.; Hires, S. A.; Looger, L. L. An optimized fluorescent probe for visualizing glutamate neurotransmission. *Nat. Methods* **2013**, *10* (2), 162−70.

(49) Jensen, T. P.; Zheng, K.; Cole, N.; Marvin, J. S.; Looger, L. L.; Rusakov, D. A. Multiplex imaging relates quantal glutamate release to presynaptic $Ca^{2+}$ homeostasis at multiple synapses in situ. *Nat. Commun.* **2019**, *10* (1), 1414.

(50) Sylantyev, S.; Savtchenko, L. P.; Niu, Y. P.; Ivanov, A. I.; Jensen, T. P.; Kullmann, D. M.; Xiao, M. Y.; Rusakov, D. A. Electric fields due to synaptic currents sharpen excitatory transmission. *Science* **2008**, *319* (5871), 1845−9.

(51) Mash, D. C.; Flynn, D. D.; Potter, L. T. Loss of $M_2$ muscarine receptors in the cerebral cortex in Alzheimer's disease and experimental cholinergic denervation. *Science* **1985**, *228* (4703), 1115−7.

(52) Zemek, F.; Drtinova, L.; Nepovimova, E.; Sepsova, V.; Korabecny, J.; Klimes, J.; Kuca, K. Outcomes of Alzheimer's disease therapy with acetylcholinesterase inhibitors and memantine. *Expert opinion on drug safety* **2014**, *13* (6), 759−74.



https://dx.doi.org/10.1021/acs.nanolett.9b04877
*Nano Lett.* XXXX, XXX, XXX−XXX

(53) Ashford, J. W. Treatment of Alzheimer's disease: the legacy of the cholinergic hypothesis, neuroplasticity, and future directions. *J. Alzheimer's Dis.* **2015**, *47* (1), 149−56.
(54) Simic, G.; Leko, M. B.; Wray, S.; Harrington, C. R.; Delalle, I.; Jovanov-Milosevic, N.; Bazadona, D.; Buee, L.; de Silva, R.; Di Giovanni, G.; Wischik, C. M.; Hof, P. R. Monoaminergic neuropathology in Alzheimer's disease. *Prog. Neurobiol.* **2017**, *151*, 101−138.
(55) Mather, M.; Harley, C. W. The locus coeruleus: essential for maintaining cognitive function and the aging brain. *Trends Cognit. Sci.* **2016**, *20* (3), 214−226.
(56) Aston-Jones, G.; Cohen, J. D. An integrative theory of locus coeruleus-norepinephrine function: Adaptive gain and optimal performance. *Annu. Rev. Neurosci.* **2005**, *28*, 403−450.
(57) Scammell, T. E.; Arrigoni, E.; Lipton, J. O. Neural circuitry of wakefulness and sleep. *Neuron* **2017**, *93* (4), 747−765.
(58) McKhann, G. M.; Knopman, D. S.; Chertkow, H.; Hyman, B. T.; Jack, C. R., Jr.; Kawas, C. H.; Klunk, W. E.; Koroshetz, W. J.; Manly, J. J.; Mayeux, R.; Mohs, R. C.; Morris, J. C.; Rossor, M. N.; Scheltens, P.; Carrillo, M. C.; Thies, B.; Weintraub, S.; Phelps, C. H. The diagnosis of dementia due to Alzheimer's disease: recommendations from the National Institute on Aging-Alzheimer's Association workgroups on diagnostic guidelines for Alzheimer's disease. *Alzheimer's Dementia* **2011**, *7* (3), 263−9.
(59) Williams, M. J.; Adinoff, B. The role of acetylcholine in cocaine addiction. *Neuropsychopharmacology* **2008**, *33* (8), 1779−97.
(60) Grace, A. A. Dysregulation of the dopamine system in the pathophysiology of schizophrenia and depression. *Nat. Rev. Neurosci.* **2016**, *17* (8), 524−32.
(61) Bast, N.; Poustka, L.; Freitag, C. M. The locus coeruleus-norepinephrine system as pacemaker of attention - a developmental mechanism of derailed attentional function in autism spectrum disorder. *European Journal of Neuroscience* **2018**, *47* (2), 115−125.
(62) Giorgi, F. S.; Pizzanelli, C.; Biagioni, F.; Murri, L.; Fornai, F. The role of norepinephrine in epilepsy: from the bench to the bedside. *Neurosci. Biobehav. Rev.* **2004**, *28* (5), 507−24.
(63) Platt, B.; Riedel, G. The cholinergic system, EEG and sleep. *Behav. Brain Res.* **2011**, *221* (2), 499−504.
(64) Ballinger, E. C.; Ananth, M.; Talmage, D. A.; Role, L. W. Basal forebrain cholinergic circuits and signaling in cognition and cognitive decline. *Neuron* **2016**, *91* (6), 1199−218.
(65) Weinshenker, D. Long road to ruin: noradrenergic dysfunction in neurodegenerative disease. *Trends Neurosci.* **2018**, *41* (4), 211−223.
(66) Ravindran, L. N.; Stein, M. B. The pharmacologic treatment of anxiety disorders: a review of progress. *J. Clin. Psychiatry* **2010**, *71* (7), 839−54.
(67) Higley, M. J.; Picciotto, M. R. Neuromodulation by acetylcholine: examples from schizophrenia and depression. *Curr. Opin. Neurobiol.* **2014**, *29*, 88−95.
(68) Gold, P. W. The organization of the stress system and its dysregulation in depressive illness. *Mol. Psychiatry* **2015**, *20* (1), 32−47.
(69) Kruse, A. C.; Kobilka, B. K.; Gautam, D.; Sexton, P. M.; Christopoulos, A.; Wess, J. Muscarinic acetylcholine receptors: novel opportunities for drug development. *Nat. Rev. Drug Discovery* **2014**, *13* (7), 549−60.
(70) Soreq, H. Checks and balances on cholinergic signaling in brain and body function. *Trends Neurosci.* **2015**, *38* (7), 448−58.
(71) Wood, S. K.; Valentino, R. J. The brain norepinephrine system, stress and cardiovascular vulnerability. *Neurosci. Biobehav. Rev.* **2017**, *74*, 393−400.
(72) Dantzer, R. Neuroimmune interactions: from the brain to the immune system and vice versa. *Physiol. Rev.* **2018**, *98* (1), 477−504.
(73) Berger, M.; Gray, J. A.; Roth, B. L. The expanded biology of serotonin. *Annu. Rev. Med.* **2009**, *60*, 355−66.


https://dx.doi.org/10.1021/acs.nanolett.9b04877
*Nano Lett.* XXXX, XXX, XXX−XXX